Analyst

PAPER

View Article Online
View Journal | View Issue

Cite this: *Analyst*, 2014, **139**, 4924

Low cost referenced luminescent imaging of oxygen and pH with a 2-CCD colour near infrared camera†

Josef Ehgartner, Helmar Wiltsche, Sergey M. Borisov and Torsten Mayr*

A low cost imaging set-up for optical chemical sensors based on NIR-emitting dyes is presented. It is based on a commercially available 2-CCD colour near infrared camera, LEDs and tailor-made optical sensing materials for oxygen and pH. The set-up extends common ratiometric RGB imaging based on the red, green and blue channels of colour cameras by an additional NIR channel. The hardware and software of the camera were adapted to perform ratiometric imaging. A series of new planar sensing foils were introduced to image oxygen, pH and both parameters simultaneously. The used NIR-emitting indicators are based on benzoporphyrins and aza-BODIPYs for oxygen and pH, respectively. Moreover, a wide dynamic range oxygen sensor is presented. It allows accurate imaging of oxygen from trace levels up to ambient air concentrations. The imaging set-up in combination with the normal range ratiometric oxygen sensor showed a resolution of 4–5 hPa at low oxygen concentrations (<50 hPa) and 10–15 hPa at ambient air oxygen concentrations; the trace range oxygen sensor (<20 hPa) revealed a resolution of about 0.5–1.8 hPa. The working range of the pH-sensor was in the physiological region from pH 6.0 up to pH 8.0 and showed an apparent pK_a-value of 7.3 with a resolution of about 0.1 pH units. The performance of the dual parameter oxygen/pH sensor was comparable to the single analyte pH and normal range oxygen sensors.

Received 2nd May 2014
Accepted 2nd July 2014

DOI: 10.1039/c4an00783b

www.rsc.org/analyst

Introduction

Since the ancestor of modern cameras, an ancient device called camera obscura, photography and imaging have had a significant impact on human lives. The progress in camera technology, especially the development of digital cameras expanded our options and made the information of an image easily accessible. In the last decades, it was demonstrated that the combination of camera technology and optical chemical sensors leads to powerful systems to image and quantify analytes by luminescence measurements.[1–6] The concentration of analytes is usually accessed by intensity-based imaging, referenced intensity-based imaging (= ratiometric imaging) or *via* imaging of luminescence lifetime.[7] Intensity based imaging is the simplest form. There, the analyte concentration causes a change in the luminescence intensity of an optical sensor and this change is recorded by the imaging set-up. Unfortunately, this change also depends on other parameters, for example heterogeneity of the light source, sensitivity of the photodetector or homogeneity of the sensor layer, which can lead to measurement inaccuracies. Some of these errors are referenced out by ratiometric imaging[8–12] due to an additional measurement of an analyte-independent (= reference) luminescence intensity signal. Yet, leaching and bleaching of the sensor material are not referenced out, but these properties can be minimized by well-engineered sensor materials. A variation of ratiometric imaging is red-green-blue (RGB) imaging, which uses standard digital photographic cameras as readout and has been used for various types of sensors.[13–17] These cameras are normally sensitive in the visible range of the spectrum and an image usually consists of the blue, green and red channel of the camera. These channels can be split up and used for ratiometric imaging. Luminescent lifetime imaging set-ups[18–21] offer an even more robust imaging system, but are much more expensive than ratiometric imaging platforms.[22]

Ratiometric imaging systems combined with optical chemical sensors were used to measure oxygen partial pressure (pO_2) in tumour tissue,[23,24] in cancer cells,[25] in neurospheres,[26] in microfluidic channels[27,28] and marine sediments,[16,29] to monitor the pH value during cutaneous wound healing processes[30] or to determine the intracellular pH value.[31] Other analytes such as glucose,[11] H_2O_2,[32,33] CO_2,[34,14] heavy metal ions[35–37] or temperature[38,39] were also determined by these techniques. Many of these imaging set-ups are optimized for the visible range and near infrared (NIR) emitting dyes are often not suitable due to low quantum efficiency of the photodetector in the near

Institute of Analytical Chemistry and Food Chemistry, Graz University of Technology, Stremayrgasse 9/3, Graz, Austria. E-mail: torsten.mayr@tugraz.at; Fax: +43 (0) 316 873 32502; Tel: +43 (0) 316 873 32504

† Electronic supplementary information (ESI) available. See DOI: 10.1039/c4an00783b

infrared or because of NIR cut-off filters in front of the photodetector. Nevertheless, the use of NIR sensors can be beneficial for example in tissue monitoring[24,25] due to a higher penetration depth of the excitation and emission light or because of less background luminescence from proteins and other cell constituents. NIR-emitting sensors are excited with red light, which has less energy than UV, blue or green light and is therefore less harmful to cells. The NIR part of the electromagnetic spectrum can also provide a window for measuring additional parameters. The purpose of our current work was the development of a low cost ratiometric imaging system for NIR sensors.[40–46] Hence, we adapted the hardware and software of a commercially available 2-CCD NIR-colour (RGB) camera to obtain a simple, more powerful and cheap set-up for referenced luminescence imaging in the visible and NIR. In addition, we developed ratiometric NIR-sensor foils for imaging of oxygen partial pressure, the pH value and simultaneous detection of pO_2 and pH. In contrast to common ratiometric RGB imaging systems our ratiometric imaging set-up has the advantage that the detection of two analytes and a reference or three analytes is easily accessible due to the additional NIR-CCD chip. Further, the 2-CCD set-up allows ratiometric imaging simultaneously in the visible and in the NIR. The two separate CCD chips do not spectrally overlap like the blue, green and red channels of RGB systems and therefore, the reference and the analyte signal can be recorded independently from each other for single analyte measurements. The spectral overlap in common RGB set-ups usually reduces the sensitivity and the dynamic range of an optical chemical sensor.

Experimental

Materials

Palladium(II) and platinum(II) *meso*-tetra(4-fluorophenyl) tetrabenzoporphyrin (PdTPTBPF and PtTPTBPF, respectively, Fig. 1), 2,3-bis(3,3,9,9-tetramethyl-2-hydroxyjulolidine)but-2-enedinitrile (BTMHJBN), the BF_2 chelate of [5-(4-hydroxyphenyl)-3-phenyl-1*H*-pyrrol-2-yl]-[5-phenyl-3-phenyl-pyrrol-2-ylidene]amine (aza-BODIPY) and 2′,7′-dichloro-5(6)-*N*-octadecyl-carboxamidofluorescein (DClFA) were synthesized in house according to the literature procedures.[44–47] Platinum(II)-5,10,15,20-tetrakis-(2,3,4,5,6-pentafluorphenyl)-porphyrin (PtTFPP) was obtained from Frontier Scientific (http://www.frontiersci.com); Macrolex Fluorescence yellow® (MFY, (3-(5-chloro-2-benzoxazolyl)-7-(diethylamino)-2*H*-1-benzo-pyran-2-one) was purchased from Simon and Werner GmbH (http://www.simon-und-werner.de); fluorescent pigment Brick red was bought from Kremer Pigmente GmbH & Co KG (http://www.kremer-pigmente.com); polyurethane hydrogel (Hydromed D4) was obtained from AdvanSource biomaterials (http://www.advbiomaterials.com); polystyrene (PS; $M = 250\,000$) was purchased from Fisher Scientific (http://www.fishersci.com). Chloroform, toluene, ethanol, sodium chloride, acetic acid and the buffer salts 2-(cyclohexylamino)ethanesulfonic acid (CHES) and 2-(*N*-morpholino)ethanesulfonic acid (MES) were purchased from Roth (http://www.carl-roth.de); tetrahydrofuran and the buffer salt 3-morpholinopropane-1-sulfonic acid (MOPS); polystyrene beads (2% divinylbenzene, 8 μm) were obtained from Sigma Aldrich (http://www.sigmaaldrich.com). Polyethylene terephthalate films (thickness 0.125 mm) were bought from Goodfellow (http://www.goodfellow.com); Teflon® AF 1600 was obtained from DU Pont (http://www.dupont.com); poly(phenylsilsesquioxane) was purchased from ABCR (http://www.abcr.de). Gases for calibration were obtained from Linde (http://www.linde-gas.at).

Preparation of the oxygen sensitive polystyrene particles

A solution of 5 mg of PtTPTBPF in 1 ml of chloroform was added dropwise to the dispersion of 1 g of polystyrene particles in 5 ml of chloroform. The dispersion was stirred at 55 °C for 30 min. It was cooled to room temperature and 1.5 ml of ethanol were added dropwise into the stirred dispersion. The particles were

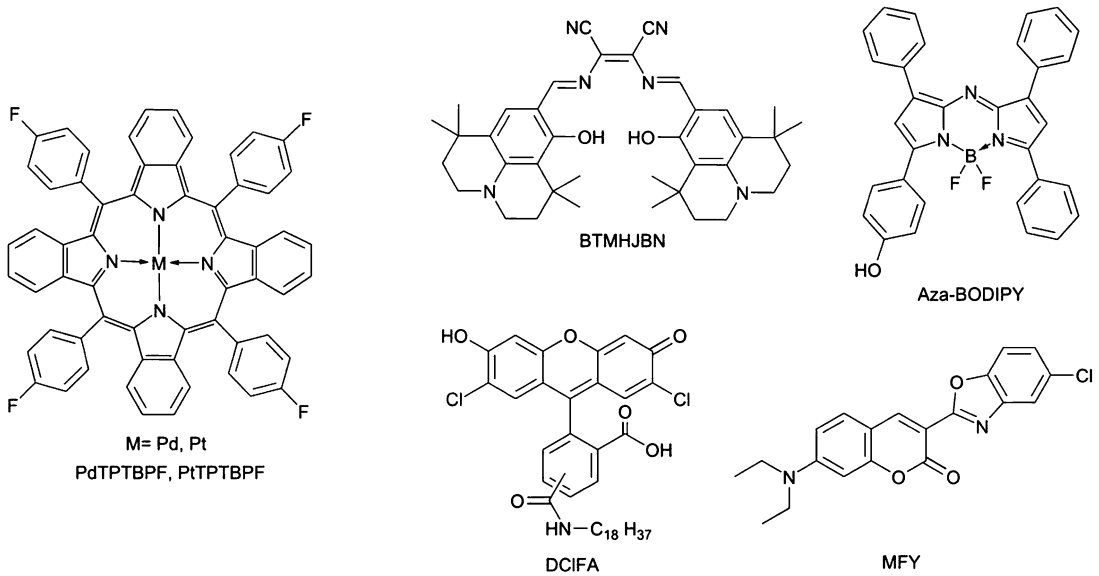

Fig. 1 Chemical structures of the indicator and reference dyes.

dried at 50 °C and homogenized in a mortar. The dye absorbed on the surface of the beads was removed by washing 4 times with 40 ml of ethanol.

Preparation and calibration of sensor films for the determination of oxygen

A sensor dye, a reference dye and polystyrene were dissolved in chloroform to obtain a sensor "cocktail". This "cocktail" (150 μl) was knife coated onto dust-free polyethylene terephthalate films by using a bar film applicator (25 μm, http://www.byk.com). The solvent was evaporated in a drying oven at 60 °C to result in an about 2.0 μm thick sensor film. The used dyes and the initial masses of all components are shown in Table 1.

A second layer of an oxygen trace sensor was spin-coated onto the PtTFPP/MFY layer to obtain a wide dynamic range oxygen sensor. For the second layer PdTPTBPF (10 mg) and poly-(phenylsilsesquioxane) (1 g) were dissolved in chloroform (3 ml). The solvent was evaporated under a nitrogen gas stream overnight and the mixture was sintered at 170 °C for four hours in an oven. The sinter was suspended in water–ethanol (4 + 1 v/v) and was ground in a ball mill (6 hours; 400 rpm). The powder was dried overnight in an oven and a portion (82 mg) was suspended in perfluorodecalin (1.2 g) containing 5% of the fluoropolymer Teflon® AF 1600. This mixture (350 μl) was spin-coated for 30 s at 3000 rpm onto the PtTFPP/MFY film by the spin coater WS-650-23NPP Modular Spin Processor (http://www.laurell.com). The solvent was evaporated in a drying oven at 60 °C. For a schematic pattern of the sensor foils see the ESI.†

Three foils of each sensor film were calibrated. The sensors PtTPTBPF/MFY, PdTPTBPF/MFY and PtTFPP/MFY/PdTPTBPF were gas-phase calibrated in a home-made calibration chamber. PtTPTBPF/BTMHJBN was calibrated in a glass vessel sealed with a lid and filled with water. Two mass flow controller instruments (Read Y smart series) by Vögtlin instruments (http://www.voegtlin.com) were used to obtain gas mixtures of defined pO_2. Compressed air and nitrogen or 2% (v/v) oxygen in nitrogen and nitrogen were used as calibration gases. The calibration gas was passed through a glass gas washing bottle (filled with wet silica gel) which was dipped into a temperature-controlled (25 °C) water bath to keep the temperature constant. The exact oxygen concentration and the temperature in the calibration vessel were determined with an optical oxygen meter (FireStingO2) from Pyroscience connected to a fiber-optic oxygen sensor and a temperature sensor (http://www.pyro-science.com). The sensors with Macrolex Fluorescence yellow® as reference dye were excited with a 458 nm high power 10 W LED array (http://www.led-tech.de). The filter set consisted of the excitation filter BG12 (350–470 nm) and the long-pass emission filter OG515 (515 nm) from Schott (http://www.schott.com). The Lee filter Oklahoma yellow (http://www.edmundoptics.com) was fixed in front of the OG515 filter to reduce its fluorescence and the background signal. The sensor with BTMHJBN as reference dye was excited with a 617 nm high power 30 W LED array (http://www.led-tech.de). The filter set consisted of the band-pass excitation filter Bk 620/25 (http://www.interferenzoptik.de) and the long-pass emission filter edge basic® 633 LP (http://www.semrock.com). The Lee filter Medium red was fixed in front of the long-pass emission filter to reduce its fluorescence and the background signal.

Table 1 Input masses of the sensor "cocktails"

Sensor dye/mg	Ref. dye/mg	Polystyrene/mg	Chloroform/g
PtTPTBPF/1.3	MFY/3.1	160	2.1
PdTPTBPF/1.0	MFY/1.1	100	1.4
PtTPTBPF/1.0	BTMHJBN/1.1	200	2.9
PtTFPP/0.9	MFY/0.3	270	2.7

Preparation and calibration of pH planar optodes

BTMHJBN (0.5 mg) as reference dye and polystyrene (500 mg) were dissolved in toluene (2.7 g). This mixture (350 μl) was spin-coated for 30 s at 3000 rpm onto a dust-free polyethylene terephthalate film by a spin coater. The solvent was evaporated in a drying oven at 70 °C. The dried reference layer was covered with a pH-sensor layer by spin coating. Hence, a pH indicator (1.0 mg)—aza-BODIPY—was dissolved in 100 μl of THF and was diluted with an ethanol + water 9 + 1 (w/w, 2.2 g) mixture containing 10% w/w hydrogel D4. 350 μl of this sensor "cocktail" were spin-coated onto the reference layer as described above. The solvents were evaporated in a drying oven at 70 °C (for schematic drawing of the sensor foil see ESI†).

Three foils of the pH sensor were calibrated; therefore, buffer solutions (MES, MOPS, CHES) at different pH values were used. The buffers were adjusted to constant ionic strength (IS = 0.15 M) using sodium chloride as a background electrolyte. The pH of the buffer solutions was controlled by a digital pH meter (SevenEasy, Mettler-Toledo, http://www.mt.com) equipped with a glass electrode (InLab Routine Pro, Mettler-Toledo). The glass electrode was calibrated with standard buffers of pH 4.1, pH 7.1 and pH 10.1 (Hanna instruments, http://www.hannainst.com). A Petri dish was used as the calibration vessel. A 617 nm high power 30 W LED array was used as the excitation source. The filter set consisted of the band-pass excitation filter bk 620/25 and the long-pass emission filter edge basic® 633 LP (http://www.semrock.com). The Lee filter Medium red was fixed in front of the long-pass emission filter to reduce its fluorescence and the background signal.

Preparation of sensor films for the simultaneous determination of oxygen and the pH value

The pH indicator DClFA (0.8 mg), polystyrene particles containing 1% w/w PtTPTBPF as the oxygen indicator (130 mg), fluorescent pigment Brick red (7.8 mg) as reference particles and ethanol + water 9 + 1 (w/w, 1.5 g) containing 15% w/w hydrogel D4 were mixed to obtain a sensor "cocktail". 150 μl of this "cocktail" were knife coated onto dust-free polyethylene terephthalate films by using a bar film applicator (25 μm). The solvent was evaporated in a drying oven at 60 °C to result in a *ca.* 3.8 μm thick sensor film (schematic drawing of the sensor foil see ESI†).

Three foils of the oxygen/pH sensor were fixed in a glass vessel and sealed with a lid. The pH value was adjusted by different buffer solutions (acetic acid–sodium acetate, MES, MOPS, CHES) and the oxygen concentration was regulated by bubbling mixtures of compressed air and nitrogen at different ratios through the solution. The pH values of the buffer solutions were controlled as described above. The oxygen mixtures were obtained by two mass flow controller instruments. The oxygen concentration and the temperature within the buffer solution were monitored online with an optical oxygen meter. A 458 nm high-power 10 W LED array was used as an excitation source. The filter set consisted of the excitation filter BG12 and the long-pass emission filter OG515. The Lee filter Oklahoma yellow was fixed in front of the OG515 filter to reduce its fluorescence and the background signal.

Spectral measurements

Emission spectra were acquired on a Hitachi F-7000 fluorescence spectrometer (http://www.hitachi-hta.com) equipped with a red-sensitive photomultiplier tube (PMT) R 928 from Hamamatsu (http://www.hamamatsu.com). The emission spectra were corrected for the sensitivity of the PMT.

Imaging set-up and data evaluation

The imaging set-up consisted of a commercial RGB-NIR camera Jai AD-130GE (http://www.jai.com) equipped with a 6 mm focal length chromatic aberration corrected lens (CVO GMHR3D26018C, http://www.stemmer-imaging.de), an LED array, optical filters and a sensor foil (Fig. 2). The software platform common vision blox (CVB 2011) from Stemmer Imaging was used to adapt the measuring software. More details and the source code of the program can be found in the supplementary information. An external trigger source was built using the Arduino open source microcontroller platform (http://www.arduino.cc) to extent the exposure time of the camera up to two seconds (more details see ESI†). The current fed to the LED array was also microcontroller adjusted by means of a field effect transistor (FET) operated in linear mode. Contrary to pulse width modulation, this linear current regulation avoided additional flicker noise in the case of very short CCD exposure time.

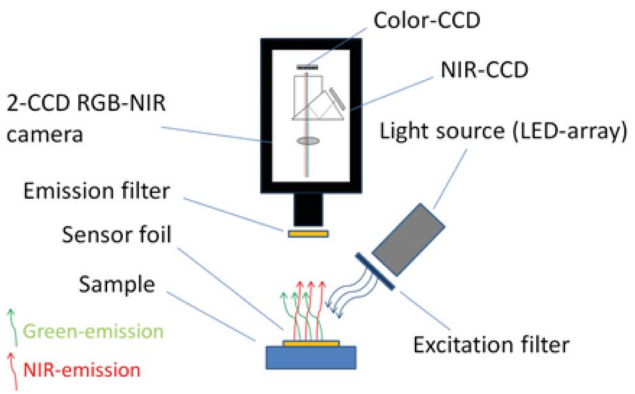

Fig. 2 Schematic drawing of the imaging set-up.

During data acquisition, two images were recorded by the camera under continuous excitation of the sensor foil. Low ambient light conditions were necessary during acquisition to minimize the background signal. One image contained the near infrared information and the other image contained the colour information (channel). The images had a size of 1296 (h) × 966 (v) pixels at 12 bit resolution which is equivalent to 4096 grey-scale values. The colour channel was separated into a blue, green and red channel each also comprising of 12 bit signal information. A ratiometric image R was obtained by dividing the channel containing the analyte dependent signal, for example the near infrared channel, by the channel containing the reference (analyte independent) signal, for example the green channel. This process was done pixel by pixel by a self-written Matlab script; therefore, each pixel contained referenced information about the analyte. Matlab R2009a (http://www.mathworks.com) was used for image processing. Also NIR and colour blank-images were recorded. These images were acquired under identical acquisition parameters (*e.g.* shutter time, brightness of the LED array *etc.*) but without a sensor foil to obtain the background signal of the measurement conditions. These background signals were subtracted from the recorded images. Calibration curves were obtained by calculating the mean value and the standard deviation of a certain region of pixels (region of interest) of a referenced image at different analyte concentrations. Fitting of the calibration data was performed using OriginLab 8.5 (http://www.originlab.com).

Results and discussion

Imaging set-up for ratiometric imaging

The main component of the detection system is the camera Jai AD-130GE, which contains two 1/3″ CCD chips. One chip is sensitive in the visible region of the spectrum and contains the blue, green and red channel (Bayer colour filter array) and the other chip is sensitive in the NIR region and contains the NIR channel. The spectral response of the camera is shown in Fig. 3. Special lenses should be used with this camera to minimize the chromatic aberration. A ratiometric optical sensor usually consists of an analyte indicator dye and an analyte independent reference dye; hence, this camera is ideally suited for ratiometric imaging due to its ability of recording the analyte signal and the reference signal in separate channels or chips of the camera. The two chip set-up provides distinct advantages over common one chip RGB systems. In comparison to the detection with monochrome cameras the 2-CCD system does not need additional equipment and moving parts, for example a filter wheel or a slider. Moreover, the NIR-chip offers an additional window for the determination of further analytes. Three-analyte detection can be performed by simultaneous detection of a reference and two analyte indicators on the RGB-chip and of an additional analyte indicator on the NIR-chip. Compared to RGB systems the 2-CCD camera is better suited for the detection of NIR-emitting optical chemical sensors. These novel sensors are beneficial in applications such as tissue monitoring or imaging of cells and biofilms in order to reduce the inherent background luminescence from biological material and from the surrounding

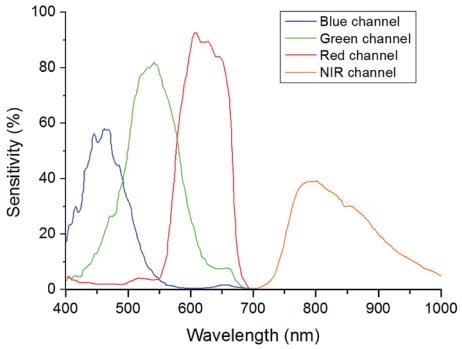

Fig. 3 Spectral response of the camera and the 4-channels adapted from Jai (http://www.jai.com).

medium itself; *e.g.* common cell culture media show strong autofluorescence in the visible part of the electromagnetic spectrum. Another advantage is the increased penetration depth into the tissue of the red excitation light of NIR emitting dyes, which is important in medical applications such as imaging of organs.

Further, the exposure time of the 2-CCD camera can be set individually for each chip and thus can be used to optimize the signals based on the brightness of the dyes if the reference and the analyte signal are recorded on separate chips. In one chip systems, for example RGB imaging, the adjustment will always be a compromise since the brightness of individual indicators may vary significantly and can only be achieved by changing the concentrations of the dyes within the sensor film. Another advantage of two chip cameras is that they offer more flexibility for the used sensor dyes. Dyes for a ratiometric imaging system must match the spectral properties of the camera. When using one chip imaging systems, the emission of a dye often overlaps with two, rather than one, channel of interest and therefore the analyte signal or the reference signal or both are influenced by each other. This property can make quantification difficult or even impossible. In one chip systems, this spectral overlap often leads to decreased sensitivity and to a narrower dynamic range of an optical chemical sensor. The used two chip camera offers more opportunities as a reference signal and an analyte signal of a sensor can be detected on independent chips without overlaps. In principle, spectral interference can be minimized or eliminated by using dedicated band-pass filters for each luminescent component. However, in order to enable fast measurements fast moving mechanical parts (filter–wheels) are essential. This results in high equipment costs (approx. 5 times higher than the dual chip camera). Our ratiometric imaging set-up consists of rather simple and cost-efficient instrumentation (approx. 3000 €) and offers in contrast to intensity-based imaging the advantage of compensating some disturbing effects for example heterogeneous thickness of the sensor films or the inhomogeneity of the light source. Fig. 4 illustrates these effects; the NIR intensity of a sensor foil over a certain region of pixels shows a drift and the signal dynamic at two different analyte concentrations changes within the intensity image (left), while the referenced value R (NIR intensity/green intensity) and the signal dynamic of this region remains constant (right) for the

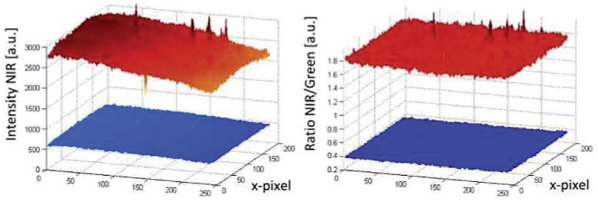

Fig. 4 Comparison of a pixel area recorded by intensity based imaging (left) and ratiometric imaging (right).

ratiometric image. Calibration of the sensor foil based on the intensity image is thus prone to error compared to the referenced image. Evidently, slight changes in the position of the camera and excitation source will negatively affect the intensity-based measurement. For accurate ratiometric measurements a constant ratio of the dyes within the sensor film is required; thus, the sensor foils must be homogeneous. In addition, scratches in the sensor foil can lead to errors due to interferences by refraction (a wavelength-dependent effect). Another source of error could be introduced by the measured sample itself if the sample randomly changes the ratio of the detected intensities by heterogeneous absorption or intrinsic luminescence.[7]

Sensor films for imaging of pO_2

Common optical oxygen sensors have limited dynamic ranges and show either a good resolution at low oxygen concentrations or at high oxygen concentrations. In some applications, *e.g.* imaging of biofilms, it might be useful to have a sensor with a wider dynamic range. Therefore, a wide dynamic range sensor was developed to image oxygen at trace levels and at ambient air conditions or even above. The advantage of this sensor over common oxygen sensors is the improved resolution for oxygen over the whole calibration range. The wide dynamic range sensor is composed of two sensing layers. The lower layer consisted of platinum(II)-5,10,15,20-tetrakis-(2,3,4,5,6-pentafluorphenyl)-porphyrin (PtTFPP) as the oxygen indicator dye and the commercially available coumarin Macrolex Fluorescence Yellow® (MFY), both dyes were incorporated into a polystyrene film. PtTFPP emitted in the red channel of the camera and MFY emitted in the green camera channel. The upper layer consisted of poly(phenylsilsesquioxane) particles with physically entrapped palladium(II) *meso*-tetra(4-fluorophenyl) tetrabenzo-porphyrin (PdTPTBPF) incorporated into a fluoropolymer film. PdTPTBPF offers the advantages that it emits in the NIR, is excitable with blue or red light and is very photostable.[48] The combination of poly(phenyl-silsesquioxane) and PdTPTBPF acts as an oxygen trace sensor within the wide dynamic range sensor because poly(phenyl-silsesquioxane) is highly permeable to oxygen and PdTPTBPF is highly sensitive to oxygen due to its long luminescence decay time ($\tau_0 \sim 350$ μs at 25 °C). The emission of MFY in the green channel of the camera was used as the reference signal for both oxygen indicators. Single layer systems were developed to offer even more accessible and more reproducible ratiometric optical oxygen sensors and to show the performance of the camera. Single layer systems usually show better

homogeneity than dual layer systems and are easier to prepare. The single layer systems used either PdTPTBPF or platinum(II) *meso*-tetra(4-fluorophenyl) tetrabenzo-porphyrin (PtTPTBPF) as oxygen indicator dye. The oxygen sensitive dye was incorporated with MFY into a polystyrene film. PdTPTBPF was used to determine oxygen at trace levels and PtTPTBPF (which has significantly shorter luminescence decay times) to detect oxygen up to air saturation and above (normal range oxygen sensor). PtTPTBPF and PdTPTBPF offer the advantages that they are excitable with blue or red light, emit in the NIR and are very photostable.[48] These ratiometric single layer systems were excitable with blue light, which in some applications can cause a higher background fluorescence and therefore another system was introduced which uses 2,3-bis(3,3,9,9-tetramethyl-2-hydroxy-julolidine)but-2-enedinitrile (BTMHJBN) as a red-excitable reference dye.[45] Its fluorescence was detected in the red channel of the camera. The oxygen indicator and the reference dye were also incorporated into a single polystyrene layer.

The spectra and Stern–Volmer calibration curves for each sensor system were recorded in triplicates and are shown in Fig. 5. Each calibration point represents the mean value of the three independent measurements and each error bar corresponds to the standard deviation. An adapted version of the two-site model, the simplified two-site model, was used to fit the calibration data (eqn (1)).[49]

$$\frac{I_0}{I} = \frac{R_0}{R} = \left(\frac{f_1}{1 + K_{SV} \cdot pO_2} + f_2\right)^{-1} \quad (1)$$

The ratio I_0/I in the model was replaced by R_0/R where R is the ratio of the measured intensity of the oxygen indicator dye divided by the intensity of the reference dye at a certain pO_2 value. R_0 represents this ratio under deoxygenated conditions, where the oxygen indicator is in its unquenched state. The parameter K_{SV} describes the quenching efficiency and thus the sensitivity of the sensor, while the parameters f_1 and f_2 characterize different fractions of dye molecules. The dye molecules in fraction f_1 are quenched at a certain K_{SV}, whereas the molecules in fraction f_2 ($f_2 = 1 - f_1$) are unquenchable ($K_{SV} = 0$).

The sensitivity (slope of the calibration curve) of the sensor system PtTPTBPF/BTMHJBN ($K_{SV} = 18.0 \times 10^{-3}$ hPa^{-1}; $f_1 = 0.996$) was slightly decreased in comparison to PtTPTBPF–MFY ($K_{SV} = 23.0 \times 10^{-3}$ hPa^{-1}; $f_1 = 0.967$), which resulted from a weak background emission of BTMHJBN in the NIR channel of the camera. The calibration parameters of the single layer trace oxygen sensor (PdTPTBPF/MFY) were $K_{SV} = 120 \times 10^{-3}$ hPa^{-1} and $f_1 = 0.913$. The calibration parameters of the dual layer system were $K_{SV} = 16.9 \times 10^{-3}$ hPa^{-1} and $f_1 = 0.734$ for the lower layer (PtTFPP/MFY) and $K_{SV} = 129 \times 10^{-3}$ hPa^{-1} and $f_1 = 0.869$ for the upper layer (PdTPTBPF entrapped into the poly-(phenylsilsesquioxane) particles). The data showed good precision as the relative standard deviation for each calibration point was within 2–5%. The sensors employing the NIR channel show a significantly higher sensitivity compared to RGB sensor systems because of recording the analyte signal and the reference signal on separate chips on the camera. Obviously, the calibration curve of the PtTFPP/MFY system of the dual sensor, which is virtually a RGB system, and the calibration curve of the PtTPTBPF/MFY dye system illustrate this and are in accordance with reported ratiometric sensor systems with a comparable sensor composition.[28] The exposure time of the NIR chip (approx. 20–30 ms) was similar for all oxygen optodes in

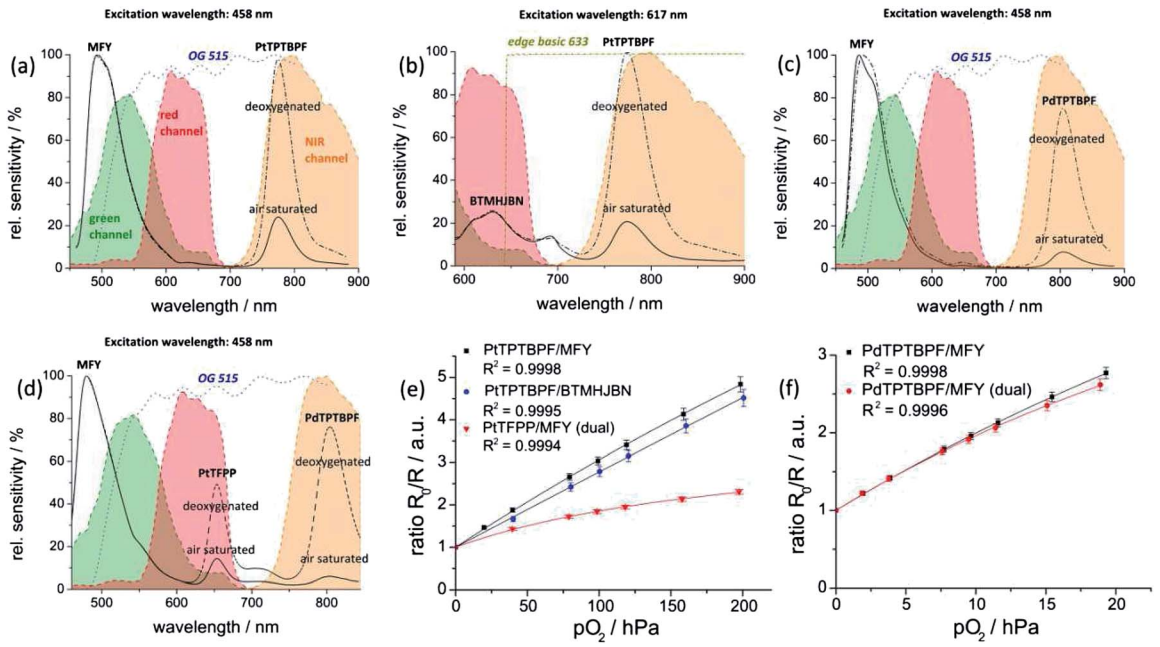

Fig. 5 Spectral properties (a–d) of the oxygen imaging set up at deoxygenated and air saturated conditions; shown are the spectral sensitivity of the camera channels, the emission spectra of the dye systems PtTPTBPF/MFY (a), PtTPTBPF/BTMHJBN (b), PdTPTBPF/MFY (c) and PtTFPP/MFY/PdTPTBPF (d) and the spectra of the emission filters (OG 515 and edge basic 633). Stern–Volmer calibration curves (e–f) for the oxygen optodes at 25 °C. Lines indicate a fit according to eqn (1).

contrast to the exposure time of the RGB chip. There, the exposure time of the red-light excitable oxygen optode (approx. 300–500 ms) had to be set five to ten times longer in comparison to the blue-light excitable system (approx. 30–50 ms) due to a lower intensity of the reference signal within the used part of the camera channel (Fig. 5). If higher signals in the red channel are needed, this can be realized either by using a shorter excitation wavelength for example an amber LED array (approx. 590 nm) in combination with a different filer set-up or by changing the ratio of the dyes within the red excitable optode.

Pseudo colour images of the near infrared intensity, of the green intensity and of the ratiometric image (each pixel represents the *R*-value) for PtTPTBPF–MFY at 0 hPa, 100 hPa and 200 hPa oxygen are shown in Fig. 6. The ratiometric images are very homogeneous in contrast to the pure intensity-based images which are very heterogeneous and thus calibration at different regions of interest would lead to different intensity values. Tiny heterogeneous areas in the ratiometric images result from small scratches of the sensor foil and wavelength-dependent diffraction of NIR and green emission light at these sides. The resolution of the imaging set-up for the normal range oxygen sensor (PtTPTBPF/MFY and PtTPTBPF/BTMHJBN) was about 4–5 hPa at a low oxygen concentration (<50 hPa) and about 10–15 hPa at ambient air oxygen concentrations; the trace range oxygen sensor (<20 hPa; PdTPTBPF/MFY) showed a resolution of about 0.5–1.8 hPa. The wide dynamic range sensor combined the beneficial behaviour of both sensor types and showed a resolution of 0.5–1.8 hPa at low oxygen concentrations (<20 hPa) and about 10–15 hPa at ambient air oxygen concentrations.

Sensor films for imaging of pH

The pH value is an important analytical parameter in many environmental systems and applications; therefore we demonstrated the applicability of our imaging set-up on a red excitable ratiometric pH sensor. As mentioned above longer excitation and emission wavelengths are beneficial because they reduce the inherent background luminescence from biological samples. Hence, the BF_2 chelate of [5-(4-hydroxyphenyl)-3-phenyl-1*H*-pyrrol-2-yl]-[5-phenyl-3-phenyl-pyrrol-2-ylidene]amine (aza-BODIPY) was used as a pH indicator dye because it emits in the NIR region, is very photostable and has high molar absorption coefficients and a good quantum yield.[46] 2,3-Bis(3,3,9,9-tetramethyl-2-hydroxyjulolidine)but-2-enedinitrile (BTMHJBN) was used as a red-light excitable reference dye, which emits in the red channel of the imaging set-up (Fig. 7). A two layer system was necessary for the sensor because the reference dye had to be incorporated into a pH insensitive matrix due to its pH sensitive hydroxyl groups; therefore polystyrene was used as a permeation selective protective matrix. The aza-BODIPY dye was immobilized in a polyurethane hydrogel D4 film upon the polystyrene layer. In two layer systems the ratio of the layer thicknesses must be similar across the imaged region; otherwise the variations of the layer thicknesses have to be determined for each pixel, which is theoretically possible but inefficient and prone to error. Spin coating was applied to obtain nearly equal distributed sensor layers.

Calibration curves of the sensor system were recorded in triplicates and are shown in Fig. 7 (mean value and standard deviation). The data were fitted by the Boltzmann function shown in eqn (2), where R is the ratio of the measured intensities of the pH indicator dye and the reference dye at a certain pH value, A_1 and A_2 represent empirical parameters describing the initial value ($A_1 = 1.244$) and the final value ($A_2 = 0.389$), x_0 describes the point of highest sensitivity (apparent pK_a value) of the sensor ($x_0 = 7.294$), and dx the pH constant of the fitting curve (d$x = 0.449$).

$$R = \frac{A_1 - A_2}{1 + \exp\left(\frac{x - x_0}{dx}\right)} + A_2 \quad (2)$$

The measurement points showed good precision as the relative standard deviation for each calibration point was within 3–4%. The ratiometric pH sensor had a working range from about pH 6.0 up to pH 8.0 and a pK_a value of 7.3, which is ideal for physiological studies. The working range of the pH sensor can be simply adjusted by using other aza-BODIPY dyes with different substitution patterns as described in the literature.[46] It should be mentioned that optical pH-sensors have a limited working range typically within 2 to 3 pH-units, which is adequate for most applications since the pH changes are typically not very high. The referenced pseudo colour images are shown in Fig. 7 and indicate a very homogeneous spatial distribution within the sensing area. The resolution of the imaging set-up and the sensor film around the apparent pK_a value was about 0.1 pH units. Further investigations will focus on the development of single layer sensor films. The reference dye might be incorporated in proton-impermeable nano- or microparticles which are dispersed in the hydrogen layer.

Sensor films for simultaneous imaging of pH and pO_2

The simultaneous detection of different analytes for example oxygen, temperature, pH, CO_2 or glucose is of great importance in order to monitor, control and understand processes of all

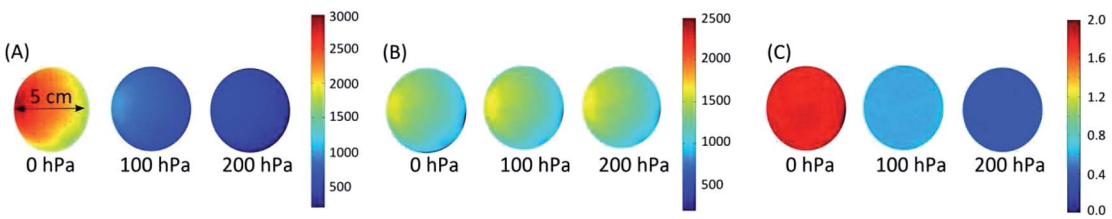

Fig. 6 Pseudo colour images of the NIR intensity channel (A), of the green intensity channel (B) and of the ratiometric images (C) at different oxygen partial pressures for the oxygen optode PtTPTBPF/MFY.

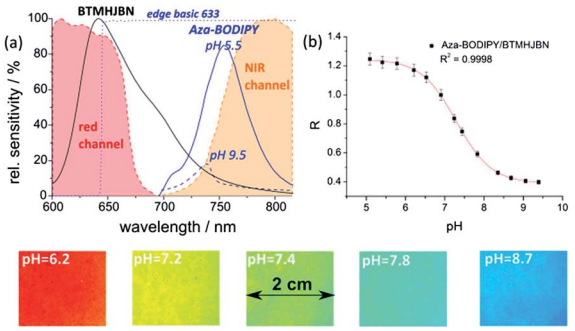

Fig. 7 Spectral properties of the pH imaging set-up at pH 5.5 and 9.5 (a); shown are the spectral sensitivity of the camera channels, the emission spectra of the used dyes (BTMHJBN and aza-BODIPY) and the spectrum of the emission filter (edge basic 633); calibration curve (b) for the pH optode at 25 °C. Lines indicate a fit according to eqn (2). Below: pseudo colour images of the referenced images of the pH sensor film at different pH values.

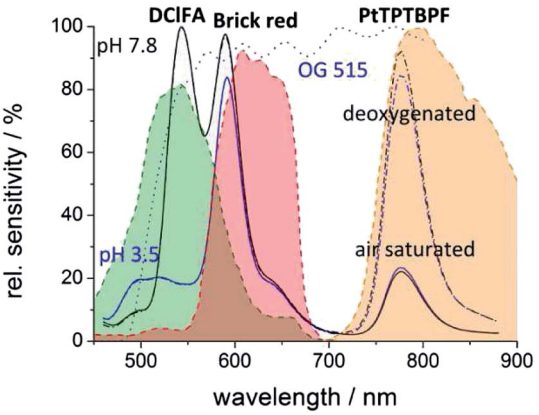

Fig. 8 Spectral properties of the dual parameter oxygen/pH sensor set-up at different pH values (3.5 and 7.8) and at different oxygen concentrations (air saturated and deoxygenated); shown are the spectral sensitivity of the camera channels, the emission spectra of the used dye system (DClFA, BrickRed and PtTPTBPF) and the spectrum of emission filters (OG 515).

kinds.[50–54] Multi-parameter detection can also be performed with the described imaging set-up and is demonstrated by an optode for simultaneous detection of the pH value and the oxygen concentration. For the pH/oxygen sensor 2′,7′-dichloro-5(6)-*N*-octadecyl-carboxamido-fluorescein (DClFA) was used as a pH indicator dye; its fluorescence was detected in the green channel of the camera. The fluorescent pigment Brick red, which emits in the red channel, was used as the reference dye; PtTPTBPF was entrapped into polystyrene particles to determine the oxygen partial pressure in the NIR channel (Fig. 8). The entrapment was performed to minimize interactions with other dyes (*e.g.* FRET). All these constituents were embedded into a hydrogel D4 matrix; the dyes are lipophilic enough not to be washed out.[52]

In comparison to single analyte sensing films, the calibration and quantification schemes of multi-parameter sensors can be more difficult as spectral overlaps of a dye with two camera channels can occur. In our system, a portion of the fluorescence of DClFA is detected in the red channel and disturbs the reference signal. This overlap does not disturb the pH measurement, but influences the oxygen detection. For the pH measurement, the ratio of the green channel (pH dependent signal) to the red channel (reference signal) changes due to this overlap, but this change is proportional to the pH value. The determined oxygen concentration in contrast would be falsified by a change of the pH value because a pH change influences the reference signal and therefore the oxygen signal even when the oxygen level stays constant. To overcome this problem, the intensity value of the red channel has to be reduced as a function of the green signal as shown in eqn (3).

$$\text{Red signal}_{\text{corrected}} = \text{red signal} - \text{green signal} \times \text{f} \qquad (3)$$

A portion (f) of the green signal which reflects the spectral overlap has to be subtracted from the red signal. This portion can be empirically determined by the use of a sensor film without a reference dye; there, the ratio of the red to the green channel reflects the spectral overlap. Calibration of the sensor at different pH values and at a certain oxygen concentration would also lead to this factor; for our multi-parameter sensor this factor was 0.245. Fig. 9 illustrates the reliability of the used correction equation. In this context, the degradation of the sensor layers by photobleaching or leaching is a critical point because these effects can change the measured signals and make the comparison of the signals with the calibration curve difficult. Hence, the indicator dyes DClFA and PtTPTBPF were chosen because of their high photostability.[55] In addition, photobleaching can be minimized by reducing the light intensity and the turn-on time of the excitation source.

Stern–Volmer calibration curves and pH calibration curves were recorded in triplicates (Fig. 9) and processed as mentioned above. The fitting parameters for the Stern–Volmer curves were $K_{SV} = 21.3 \times 10^{-3}$ hPa and $f_1 = 0.930$; the relative standard deviation for each calibration point was within 4–6%. The resolution of the oxygen sensor was 25–30 hPa at high oxygen concentrations and 6–10 hPa at low oxygen concentrations. The fitting parameters for the pH sensor were $A_1 = 0.677$ (air saturated) and 0.690 (deoxygenated), $A_2 = 1.563$ (air saturated) and 1.594 (deoxygenated), $x_0 = 6.285$ and $dx = 0.285$. The sensor had a working range of pH 5.5 to 7.0 and an apparent pK_a value of 6.3 and the resolution in the vicinity of the pK_a was about 0.1 pH units. The referenced pseudo colour images of the oxygen and pH sensor films are illustrated in Fig. 9. The oxygen images showed in comparison to single layer systems more heterogeneous areas due to a slightly unequal distribution of the oxygen particles; thus, the resolution for oxygen of the dual-parameter sensor was lower than with the single layer oxygen sensor films. The homogeneity of the pH images was comparable to the two layer system. The dual-parameter oxygen/pH sensor can be a useful tool for example in biology to image oxygen and pH distributions or changes in biofilms.

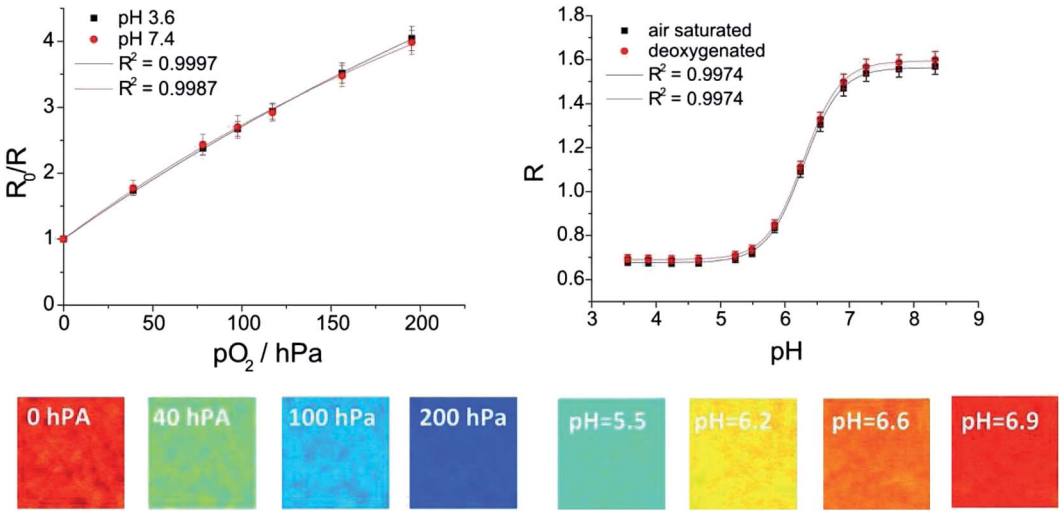

Fig. 9 Above: calibration curves of the dual-parameter oxygen/pH sensor at 21 °C. Lines indicate a fit according to eqn (1) and (2). Below: pseudo colour images of the dual-parameter oxygen/pH sensor at certain oxygen concentrations and pH values.

Conclusion

We presented a new imaging set-up for simultaneous detection of optical chemical sensors emitting in the visible and in the NIR regions of the electromagnetic spectrum. The dual chip camera offers the opportunity of two separate chips and therefore minimizes the optical cross-talk and allows real time measurements at four wavelengths (without moving parts) at low costs. The set-up is compatible with high performance NIR sensing materials allowing more reliable measurements in scattering media and biological samples because of an increased optical transparency and less autofluorescence in the NIR regime. The simultaneous determination of at least two parameters is also possible as shown with this measurement system. We demonstrated that ratiometric imaging of oxygen, pH and both parameters simultaneously can be accomplished with high accuracy by our developed optical optodes. Moreover, we developed a wide dynamic range oxygen sensor which allows accurate oxygen measurements over the whole calibration range. The imaging system can be adapted to a large variety of different optical sensors and will be applicable to many analytes and applications varying from marine science to microfluidics or biotechnology or food packaging. Ongoing investigations will focus on multi-parameter detection.

Acknowledgements

Financial support by the European Union FP7 Project BIO-INTENSE – Mastering Bioprocess integration and intensification across scales (Grant Agreement Number 312148) is gratefully acknowledged.

References

1 A. K. Kenworthy, *Methods*, 2001, **24**, 289–296.
2 S. Ke, X. Wen, M. Gurfinkel, C. Charnsangavej, S. Wallace, E. M. Sevick-Muraca and C. Li, *Cancer Res.*, 2003, **63**, 7870–7875.
3 S. A. Vinogradov, L. W. Lo, W. T. Jenkins, S. M. Evans, C. Koch and D. F. Wilson, *Biophys. J.*, 1996, **70**, 1609–1617.
4 M. Yang, E. Baranov, A. R. Moossa, S. Penman and R. M. Hoffman, *Proc. Natl. Acad. Sci. U. S. A.*, 2000, **97**, 12278–12282.
5 R. N. Glud, N. B. Ramsing, J. K. Gundersen and I. Klimant, *Mar. Ecol.: Prog. Ser.*, 1996, **140**, 217–226.
6 R. N. Glud, M. Kühl, O. Kohls and N. B. Ramsing, *J. Phycol.*, 1999, **35**, 270–279.
7 G. Liebsch, *Dissertation*, University of Regensburg, 2000.
8 Y. Cao, Y.-E. Lee Koo and R. Kopelman, *Analyst*, 2004, **129**, 745–750.
9 C. Wu, B. Bull, K. Christensen and J. McNeill, *Angew. Chem., Int. Ed. Engl.*, 2009, **48**, 2741–2745.
10 D. W. Domaille, L. Zeng and C. J. Chang, *J. Am. Chem. Soc.*, 2010, **132**, 1194–1195.
11 H. Xu, J. W. Aylott and R. Kopelman, *Analyst*, 2002, **127**, 1471–1477.
12 S. H. Im, G. E. Khalil, J. Callis, B. H. Ahn, M. Gouterman and Y. Xia, *Talanta*, 2005, **67**, 492–497.
13 D. Aigner, B. Ungerböck, T. Mayr, R. Saf, I. Klimant and S. M. Borisov, *J. Mater. Chem. C*, 2013, **1**, 5685–5693.
14 R. Ali, T. Lang, S. M. Saleh, R. J. Meier and O. S. Wolfbeis, *Anal. Chem.*, 2011, **83**, 2846–2851.
15 L. H. Fischer, C. Karakus, R. J. Meier, N. Risch, O. S. Wolfbeis, E. Holder and M. Schäferling, *Chemistry*, 2012, **18**, 15706–15713.
16 M. Larsen, S. M. Borisov, B. Grunwald, I. Klimant and R. N. Glud, *Limnol. Oceanogr.: Methods*, 2011, **9**, 348–360.
17 X.-d. Wang, H. H. Gorris, J. A. Stolwijk, R. J. Meier, D. B. M. Groegel, J. Wegener and O. S. Wolfbeis, *Chem. Sci.*, 2011, **2**, 901.

18 J. R. Lakowicz, H. Szmacinski, K. Nowaczyk, K. W. Berndt and M. Johnson, *Anal. Biochem.*, 1992, **202**, 316–330.
19 T. W. Gadella, T. M. Jovin and R. M. Clegg, *Biophys. Chem.*, 1993, **48**, 221–239.
20 (*a*) P. Hartmann and W. Ziegler, *Anal. Chem.*, 1996, **68**, 4512–4514; (*b*) P. Hartmann, W. Ziegler, G. Holst and D. W. Lübbers, *Sens. Actuators, B*, 1997, **38**, 110–115.
21 H. Stahl, A. Glud, C. R. Schröder, I. Klimant, A. Tengberg and R. N. Glud, *Limnol. Oceanogr.: Methods*, 2006, **4**, 336–345.
22 R. J. Meier, L. H. Fischer, O. S. Wolfbeis and M. Schäferling, *Sens. Actuators, B*, 2013, **177**, 500–506.
23 P. Babilas, V. Schacht, G. Liebsch, O. S. Wolfbeis, M. Landthaler, R.-M. Szeimies and C. Abels, *Br. J. Cancer*, 2003, **88**, 1462–1469.
24 J. Napp, T. Behnke, L. Fischer, C. Würth, M. Wottawa, D. M. Katschinski, F. Alves, U. Resch-Genger and M. Schäferling, *Anal. Chem.*, 2011, **83**, 9039–9046.
25 Y.-E. K. Lee, E. E. Ulbrich, G. Kim, H. Hah, C. Strollo, W. Fan, R. Gurjar, S. Koo and R. Kopelman, *Anal. Chem.*, 2010, **82**, 8446–8455.
26 R. I. Dmitriev, A. V. Zhdanov, Y. M. Nolan and D. B. Papkovsky, *Biomaterials*, 2013, **34**, 9307–9317.
27 L. Gitlin, C. Hoera, R. J. Meier, S. Nagl and D. Belder, *Lab Chip*, 2013, **13**, 4134–4141.
28 B. Ungerbock, V. Charwat, P. Ertl and T. Mayr, *Lab Chip*, 2013, **13**, 1593–1601.
29 I. Klimant, M. Kühl, R. N. Glud and G. Holst, *3rd European Conference on Optical Chemical Sensors and Biosensors*, 1997, 38, pp. 29–37.
30 S. Schreml, R. J. Meier, O. S. Wolfbeis, M. Landthaler, R.-M. Szeimies and P. Babilas, *Proc. Natl. Acad. Sci. U. S. A.*, 2011, **108**, 2432–2437.
31 H.-s. Peng, J. A. Stolwijk, L.-N. Sun, J. Wegener and O. S. Wolfbeis, *Angew. Chem.*, 2010, **122**, 4342–4345.
32 P. Niethammer, C. Grabher, A. T. Look and T. J. Mitchison, *Nature*, 2009, **459**, 996–999.
33 M. Wu, Z. Lin, M. Schäferling, A. Dürkop and O. S. Wolfbeis, *Anal. Biochem.*, 2005, **340**, 66–73.
34 G. Liebsch, I. Klimant, B. Frank, G. Holst and O. S. Wolfbeis, *Appl. Spectrosc.*, 2000, **54**, 548–559.
35 T. Mayr, C. Igel, G. Liebsch, I. Klimant and O. S. Wolfbeis, *Anal. Chem.*, 2003, **75**, 4389–4396.
36 T. Mayr, I. Klimant, O. S. Wolfbeis and T. Werner, *Anal. Chim. Acta*, 2002, **462**, 1–10.
37 M. Iniya, D. Jeyanthi, K. Krishnaveni, A. Mahesh and D. Chellappa, *Spectrochim. Acta, Part A*, 2014, **120**, 40–46.
38 H. Peng, M. I. J. Stich, J. Yu, L.-N. Sun, L. H. Fischer and O. S. Wolfbeis, *Adv. Mater.*, 2010, **22**, 716–719.
39 O. Filevich and R. Etchenique, *Anal. Chem.*, 2006, **78**, 7499–7503.
40 (*a*) I. B. Rietveld, E. Kim and S. A. Vinogradov, *Tetrahedron*, 2003, **59**, 3821–3831; (*b*) A. Y. Lebedev, A. V. Cheprakov, S. Sakadzić, D. A. Boas, D. F. Wilson and S. A. Vinogradov, *ACS Appl.Mater. Interfaces*, 2009, **1**, 1292–1304.
41 J. M. Baumes, J. J. Gassensmith, J. Giblin, J.-J. Lee, A. G. White, W. J. Culligan, W. M. Leevy, M. Kuno and B. D. Smith, *Nat. Chem.*, 2010, **2**, 1025–1030.
42 S. Sreejith, K. P. Divya and A. Ajayaghosh, *Angew. Chem., Int. Ed. Engl.*, 2008, **47**, 7883–7887.
43 S. O. McDonnell and D. F. O'Shea, *Org. Lett.*, 2006, **8**, 3493–3496.
44 S. M. Borisov, G. Zenkl and I. Klimant, *ACS Appl. Mater. Interfaces*, 2010, **2**, 366–374.
45 S. M. Borisov, R. Saf, R. Fischer and I. Klimant, *Inorg. Chem.*, 2013, **52**, 1206–1216.
46 T. Jokic, S. M. Borisov, R. Saf, D. A. Nielsen, M. Kühl and I. Klimant, *Anal. Chem.*, 2012, **84**, 6723–6730.
47 T. Matray, V. Hernandez and S. Singh, United States Patent 6,673,550, 2002.
48 S. M. Borisov, G. Nuss and I. Klimant, *Anal. Chem.*, 2008, **80**, 9435–9442.
49 J. N. Demas, B. A. DeGraff and W. Xu, *Anal. Chem.*, 1995, **67**, 1377–1380.
50 J. A. Ferguson, B. G. Healey, K. S. Bronk, S. M. Barnard and D. R. Walt, *Anal. Chim. Acta*, 1997, **340**, 123–131.
51 D. Wencel, C. Higgins, A. Klukowska, B. D. MacCraith and C. McDonagh, *Mater. Sci.-Pol.*, 2007, **25**, 767–779.
52 M. I. J. Stich, L. H. Fischer and O. S. Wolfbeis, *Chem. Soc. Rev.*, 2010, **39**, 3102.
53 B. Zelelow, G. E. Khalil, G. Phelan, B. Carlson, M. Gouterman, J. B. Callis and L. R. Dalton, *Sens. Actuators, B*, 2003, **96**, 304–314.
54 L. Li and D. R. Walt, *Anal. Chem.*, 1995, **67**, 3746–3752.
55 B. M. Weidgans, C. Krause, I. Klimant and O. S. Wolfbeis, *Analyst*, 2004, **129**, 645.